Phagophore formation by the autophagy conjugation machinery

Jagan Mohan
Institut Pasteur
Christine Girard Blanc
Institut Pasteur
Satish Moparthi
Institut Myologie
Charlotte Nugues
Institut Pasteur
Sowmya Rama
Institut Pasteur
Stéphane Vassilopoulos
Centre de Recherche en Myologie, UMRS 974 https://orcid.org/0000-0003-0172-330X
Thomas Wollert (thomas.wollert@pasteur.fr)
Institut Pasteur https://orcid.org/0000-0001-9732-4789

Biological Sciences - Article

Keywords:

Posted Date: January 25th, 2022

DOI: https://doi.org/10.21203/rs.3.rs-1269772/v1

Abstract

Autophagy is a fundamental cellular recycling pathway that captures cytoplasmic material by a phagophore membrane and delivers it to lysosomes for degradation. Nonselective phagophores are generated at specialized ER-domains termed omegasomes. Mechanistically, this process is not well understood. Here, we reconstituted the formation of phagophores from purified components on supported lipid bilayers and by ectopic induction of nonselective autophagy at the plasma membrane. We found that enzymatic conjugation of LC3B to model membranes induces the formation of phagophore-like membrane cups. LC3B functions as membrane anchor, ensuring a sustained interaction of the E3-like ligase complex ATG12¬–ATG5-ATG16L1 with membranes by forming extended membrane coats. ATG16L1 is the major membrane remodeling factor that induces positive membrane curvature, promotes cup formation and stabilizes the rim of membrane cups. Redirecting WIPI2 to the plasma membrane by expressing WIPI2-CAAX induced the formation of omegasome-like membrane cisternae to which LC3B was conjugated. Membrane cups, identical to those observed in vitro, emerged from these cisternae. ATG16L1 variants that did not induce the formation of cups in vitro also failed to promote cup formation in vivo and inhibited the biogenesis of nonselective autophagosomes in cells. We thus propose that ATG16L1 drives the formation of nonselective phagophores by shaping flat donor membranes into membrane cups.

Main Text

Macroautophagy (autophagy in the following) is a highly conserved pathway that sequesters cytoplasmic material in double-membrane bound autophagosomes and delivers it to lysosomes for degradation[1]. Autophagy maintains cellular homeostasis by degrading unwanted or damaged cytoplasmic components[2] and by recycling bulk cytoplasm during periods of nutrient deprivation or cytotoxic stresses[3]. Selective autophagy is thus tightly coupled to the presence of superfluous or damaged material, while nonselective autophagy occurs independently of specific cargo[4].

The formation of autophagosomes is driven by autophagy related (ATG) proteins that assemble at sites of phagophore formation in a highly coordinated and sequential manner. Initiation of autophagy depends on the activation of the ULK1 complex which is followed by the recruitment of the phosphatidylinositol (PtdIns)-3-kinase complex (PI3K)[5] and of ATG9 vesicles, which nucleate phagophores[6].

The expansion of phagophores depends on the mobilization of various lipid reservoirs, including organelles[7–10], lipid droplets[11] or direct lipid transfer from the ER[12]. Moreover, this process is accompanied by the conjugation of ubiquitin-like ATG8 proteins to the lipid phosphatidylethanolamine (PE)[13]. The reaction is catalyzed by a ubiquitin-like conjugation system comprising the E1 enzyme ATG7, the E2 enzyme ATG3, and an E3 ligase complex that consists of the ATG12–ATG5 conjugate and the coiled-coil protein ATG16L1[14–16]. The latter is recruited to early phagophores by the PtdIns(3)phosphate binding protein WIPI2[17].

The ATG8 family of proteins comprises microtubule-associated protein 1 light chain 3 (LC3)A, LC3B and LC3C as well as gamma-amino-butyric acid receptor-associated protein (GABARAP), GABARAPL1 and GABARAPL2. All ATG8 proteins can tether cargo to phagophore membranes in selective autophagy[4], while LC3C and GABARAPs recruit autophagosomes to lysosomes[18,19] and GABARAPs promote autophagosome-lysosome fusion[20]. LC3 proteins are dispensable for selective autophagy[20–23] but nonselective phagophores continuously acquire LC3B and the amount of LC3B correlates with the size of phagophores[24]. The molecular function of LC3B during nonselective autophagy remains, however, to be discovered.

Here, we applied an integrated and multidisciplinary approach to obtain mechanistic insights into the formation of nonselective autophagosomes. We found that LC3B cooperates with ATG12–ATG5-ATG16L1 to form protein coats that remodel flat membranes into membrane cups that resemble phagophores. ATG16L1 was particularly important by stabilizing the highly bent membrane rim of cups and by driving cup-expansion. We also found that simple lipid bilayers serve as platform for cup formation in vitro, while in cells, cups emerge only from omegasome-like membranes. ATG16L1 variants that stalled cup formation at distinct stages in vitro and in vivo also stalled the formation of nonselective autophagosomes in starved cells. We thus propose that nonselective phagophores are generated by remodeling omegasomes into membrane cups and that this process is driven by ATG161L1.

Results

LC3B and ATG12–ATG5-ATG16L1 form a protein coat on membranes in vitro

Nonselective autophagy is characterized by a marked increase in the number of LC3B-positive autophagosomes, suggesting that LC3B fulfills a particular, yet unknown function in this process. To identify novel functions of LC3B in nonselective autophagy, we conjugated LC3B to model membranes in vitro. We first purified all components of the conjugation system including the proteolytically activated form of LC3B ($LC3B^{G120}$, **Extended Data Figure 1a**) and confirmed the catalytic activity of ATG7 and ATG3 (**Extended Data Figure 1b**). We then conjugated Alexa488 labeled $LC3B^{G120}$ to Giant Unilamellar Vesicles (GUVs) using ATG7, ATG3, ATP and the E3-ligase ATG12–ATG5-ATG16L1 and followed conjugation in real time by confocal microscopy (**Supplementary Movie 1**). The fluorescence of $LC3B^{G120}$ increased over time and reached a plateau after ~80 min (Figure **1a**). Remarkedly, the conjugation reaction induced the formation of small membrane buds on GUVs (**Figure 1a**, **b**), which were initially mobile but lost mobility with increasing $LC3B^{G120}$ levels (**Figure 1c**, **Extended Data Figure 1c** and **Supplementary Movies 1 and 2**). Furthermore, small GUV-derived LC3B-positive vesicles accumulated over time, suggesting that the conjugation of LC3B to GUVs induces membrane deformations and budding (**Figure 1c** and **Extended Data Figure 1d**). To decipher whether membrane deformations depend on LC3B or ATG16L1, we conjugate LC3B to GUVs in the absence of ATG16L1 using a minimal E3-ligase complex ATG12–ATG5-$ATG16L1^{NT}$ (NT = residues 11-43)[25] since ATG12–ATG5 alone was catalytically inactive. Although

LC3B^{G120} was efficiently conjugated to GUVs, membrane deformations were not observed (**Figure 1d** and **Extended Data Figure 1g**), which is consistent with a contribution of full-length ATG16L1 (ATG16L1^{FL}) in deforming membranes[26]. Fluorescence recovery after photobleaching (FRAP) showed that fluorescent labeled LC3B^{G120} and ATG16L1^{FL} did not exchange with the bulk solution and that their lateral diffusion at the membrane was strongly attenuated (**Figure 1e** and **Extended Data Figure 1e**, **f**). However, in conjugations with ATG12–ATG5-ATG16L1^{NT}, the fluorescence of a substantial fraction of LC3B^{G120} recovered rapidly by lateral diffusion (**Figure 1f** and **Extended Data Figure 1g**). Our data suggest that LC3B and ATG12–ATG5-ATG16L1 form an immobile macromolecular complex that deforms membranes.

To study the morphology of these assemblies, we conjugated LC3B^{G120} to Supported Lipid Bilayers (SLBs), which are flat model membranes that are attached to a stiff glass support, using the full conjugation machinery including ATG12–ATG5-ATG16L1^{FL} and characterized the topology of proteins by atomic force microscopy (AFM). Before the reaction, SLBs were perfectly flat and possessed a height of 5 ± 1 nm (**Figure 1g**). Conjugating LC3B to these membranes induced the formation of a continuous protein layer with a height of 22 nm (**Figure 1h** and **Extended Data Figure 2a**) and LC3B was entirely immobilized (**Extended Data Figure 2b**), reminiscent of a protein coat. When the conjugation reaction was performed with ATG12–ATG5-ATG16L1^{NT}, no such protein coat was present. Instead, mobile particles with a mean diameter of 70 ± 10 nm and a height of 23 ± 3 were observed (**Extended Data Figure 2c**).

Given that ATG16L1 is a crucial component of the protein coat, we next identified critical domains in ATG16L1 that are required for coat formation. We first removed the C-terminal WD-domain of ATG16L1 which is known to be dispensable for canonical autophagy[27]. The corresponding ATG12–ATG5-ATG16L1^{307} complex catalyzed LC3B^{G120} lipidation and immobilized LC3B^{G120} (mobile fraction = 9 ± 5 %, **Figure 1f** and **Extended Data Figure 2d, e**). Truncation of a part of the C-terminal lipid binding domain (ATG16L1^{264})[28] impaired coat formation as evident by an increase in the mobile LC3B^{G120} fraction to 23 - ± 8 % (**Figure 1f** and **Extended Data Figure 2d, e**). An even stronger effect was observed when the entire C-terminal membrane binding domain was removed (ATG16L1^{230}, mobile fraction = 38 ± 13 %), or if only the ATG5 binding domain was left (ATG16L1^{NT}, mobile fraction = 53 ± 10 %, **Figure 1f** and **Extended Data Figure 2d, e**). In conclusion, ATG5-binding, coiled coil and membrane binding regions of ATG16L1 are required for coat formation while the WD domain is dispensable. AFM of the corresponding ATG16L1^{307} coat revealed that a less dense protein layer with striated appearance was formed (**Extended Data Figure 2f**). Furthermore, the height of this coat (11 ± 2 nm) was thinner than that formed by full-length ATG16L1. This suggests that the WD domain of ATG16L1 projects away from the membrane, while its 30 nm long coiled-coil domain aligns with the membrane. Taken together, our data reveal that LC3B recruits ATG12–ATG5-ATG16L1 to membranes at which both assemble into extended membrane coats and remodel membranes.

ATG16L1 remodels flat membranes into phagophore-like cups

As shown in Fig. 1a, the conjugation of LC3B to free standing membranes (GUVs) induced membrane budding and remodeling in an ATG16L1 dependent manner. To better define the nature of these membrane remodeling events, we established a new method that combines in vitro reconstitution and production of metal replicas for Platinum Replica Electron Microscopy (PREM). We first conjugated LC3B to SLBs using ATG12–ATG5-ATG16L1^{FL} and studied the membrane topology by PREM. We found that large areas of flat SLBs were remodeled into membrane cups that closely resembled phagophores (**Figure 2a**, **Extended Data Figure 3a** and **Supplementary Movie 3**). Most membrane cups had diameters between 150 and 300 nm and possessed a well-defined rim of 25 ± 3 nm that was covered by a dense protein coat. (**Extended Data Figure 3a** and **Supplementary Movie 3**). The striated appearance of this coat suggests that it consists of parallelly packed filamentous proteins, most likely ATG16L1. To reveal the specific contribution of ATG16L1 in the formation of membrane cups and rims, we performed reconstitutions using ATG12–ATG5-ATG16L1^{NT} that lacked most of ATG16L1. In these reactions, the integrity of SLBs was maintained, the membrane was not deformed, proteins were not dispersed on SLBs but accumulated in aggregates, leaving most of the SLB surface devoid of protein (**Figure 2b**). We next tested whether ATG16L1^{207} that contains the minimal coiled coil domain[29] promotes membrane deformations. In corresponding reconstitutions, large areas of SLBs were covered by a homogenously dispersed layer of proteins. Although some amorphous membrane deformations were observed, defined structures such as membrane cups or rims were not present (**Figure 2c**). In reconstitutions with ATG16L1^{230} comprising the full coiled-coil domain of ATG16L1 and its WIPI2 binding site[17], LC3B and the corresponding E3 ligase complex assembled into densely packed particles with a diameter of 28 ± 5 nm (Figure **2d**). Furthermore, SLBs were deformed into 100-300 nm wide rings that resembled rims of membrane cups seen in reconstitutions with full-length ATG16L1. Interestingly, a striated pattern, similar to that observed in reactions with ATG16L1^{FL}, was present on membrane rims (**Extended Data Figure 3b**). Our experiment thus demonstrates that ATG16L1^{230} deforms membranes into rims without promoting the formation of membrane cups.

A recent study reported that two isoforms of ATG16L1 are involved in distinct types of autophagy[28]. ATG16L1^{a} promotes canonical autophagy but lacks a membrane binding site that is present in ATG16L1^{b},[28]. We thus tested whether an ATG16L1 variant that contains only the conserved core region of both isoforms (ATG16L1^{264}) promotes cup formation. In reactions with ATG16L1^{264}, SLBs were also covered with distinct and well-defined particles with diameters of 39 ± 5 nm, which were bigger than particles observed in reactions with ATG16L1^{230} (**Figure 2e**). Interestingly, some of these particles were interconnected by rod-like structures (arrowheads in **Figure 2e** and **Extended Data Figure 3c**), suggesting that ATG16L1^{264} induces the formation of a loosely packed protein coat. Moreover, irregular cup-like structures were observed. The rims of these cups were sharp and covered with a striated protein coat, but mostly irregular in shape (**Figure 2e** and **Extended Data Figure 3b**), demonstrating that ATG16L1^{264} does not support the formation of fully expanded and regular membrane cups.

We next tested whether the C-terminal membrane binding region contributes to cup formation by reconstituting the reaction with ATG16L1^{307}. Indeed, mature membrane cups that closely resembled those produced by full-length ATG16L1 were observed (**Figure 2f** and **Supplementary Movie 4**). These cups had diameters of up to 300 nm and rims with a width of » 17 nm. Furthermore, SLBs were covered by distinct particles, as seen in reconstitutions with ATG16L1^{264}, but they were closely packed to form a dense, continuous protein coat (**Figure 2f**). Taken together, all ATG16L1 variants that immobilized LC3B (in FRAP experiments) and assembled into organized membrane coats (as seen in PREM) also promote the formation of membrane cups. Moreover, the morphology of membrane cups correlates with the quality of the membrane coat: fully expanded cups were generated by ATG16L1FL^{307} and ATG16L1FL^{FL} which form part of continuous membrane coats, while irregular cups and loose membrane coats are present in reactions with ATG16L1FL^{264}. By contrast, ATG16L1^{230}, which does not promote the formation of membrane coats and cups, deformed membranes into flat rims.

Reconstituting cup formation in cells

Our in vitro studies demonstrated that ATG16L1 is a major membrane remodeling protein. We thus tested whether ATG16L1 also remodels biological membranes in cells. To bypass upstream autophagy proteins, we uncoupled ATG16L1 recruitment from canonical autophagy by targeting WIPI2 to the plasma membrane (PM). We therefore co-expressed the well-established, plasma membrane-targeted WIPI2-CAAX construct that lacks its PtdIns(3)P binding site[17] with mCherry-ATG16L1 and GFP-LC3B in ATG16L1 knock-out cells. We found that WIPI2-CAAX recruited ATG16L1 and induced conjugation of LC3B to the PM (**Figure 3a**), whereas ULK1 and ATG9 remained in the cytoplasm (**Extended Data Figure 4a**). Furthermore, depletion of ULK1 by siRNA (**Figure 3b** and **Extended Data Figure 4b**) or treatment with the ULK1 inhibitor SBI-0206965 (**Extended Data Figure 4c**) did not impact on LC3B targeting. Although ATG14, a subunit of the PI3-kinase complex, was also recruited to the PM, its depletion by siRNA (**Figure 3b** and **Extended Data Figure 4a, b**) or treatment with the PI3-kinase inhibitor SAR405 (**Extended Data Figure 4c**) did not impact on PM-targeting of LC3B. Moreover, PtdIns(3)P was not detected at the PM (**Extended Data Figure 4d**) and starvation had no significant impact on the recruitment of LC3B (**Figure 3c** and **Extended Data Figure 4e**), demonstrating that recruitment of ATG16L1 and conjugation of LC3B to the PM occurs independently of the upstream autophagy machinery.

We next explored the morphology of the PM by PREM of unroofed cells expressing WIPI2-CAAX alone. Although membrane deformations or cup-like structures were not observed, we noticed the presence of extended patches of cortical endoplasmic reticulum (cER) (**Extended Data Figure 5a**). Similar cER patches were not observed in cells expressing WIPI2 without CAAX-tag (**Extended Data Figure 5b**) or in non-transfected cells (**Extended Data Figure 5c**). Furthermore, PM and cER were covered with »20 nm large, doughnut-shaped particles, corresponding most likely to WIPI2 (**Extended Data Figure 5a**). Identical particles were also present in cells that co-expressed WIPI2-CAAX and ATG16L1 (**Extended Data Figure 5d**). Characterizing the morphology of cER patches by Transmission-EM (TEM) of ultrathin cryo-sections revealed that PM and cER were tightly aligned with a constant distance of 16 ± 1 nm (**Figure 3d**, **Extended**

Data Figure 5e and **Supplementary Movie 5**). The lumen of cER was with an intermembrane distance of 24 ± 2 nm much thinner than that of canonical ER. Interestingly, ER-derived omegasomes that serve as platforms for the biogenesis of autophagosomes, possess similar characteristics with almost identical intraluminal distances[30], suggesting that WIPI2-CAAX induces the formation of omegasome-like membrane cisternae at the PM (**Fig. 3d**).

We next co-expressed WIPI2-CAAX, ATG16L1 and LC3B and investigated the morphology of the PM by PREM. We observed large membrane cups that closely resembled cups on SLBs in vitro (**Extended Data Figure 5f**). Immunogold labeling of GFP-LC3B and HA-ATG16L1 in PREM samples confirmed the presence of both proteins on such structures (**Extended Data Figure 5g**). Interestingly, membrane cups were only observed on cER and not at the PM, although WIPI2-CAAX, ATG16L1 and LC3B are recruited to both membranes (**Figure 3e** and **Supplementary Movie 6**). This suggests that the formation of membrane cups is restricted to omegasome-like membranes in vivo, while a simple lipid bilayer serves as substrate for cup formation in vitro.

We next tested whether ATG16L1 variants that stabilized cup intermediates on SLBs in vitro produced similar intermediates in vivo. We first expressed ATG16L1^{207}, which lacks the WIPI2 binding site, together with WIPI2-CAAX and LC3B in ATG16L1 knockout (KO) cells and found that ATG16L1^{207} was not recruited, LC3B was thus not conjugated and the morphology of PM and cER was unchanged (**Extended Data Figure 6a**). All other tested ATG16L1 variants contained the WIPI2 binding site and were recruited together with LC3B to the PM (**Extended Data Figure 6b**). Furthermore, ATG16L1^{230} deformed cER membranes into flat ring-like structures with diameters of 510 ± 160 nm (**Figure 3f** and **Supplementary Movie 7**) which closely resembled rings produced by ATG16L1^{230} on SLBs in vitro. Expression of ATG16L1^{264} induced the formation of irregular cups (**Figure 3g**), while ATG16L1^{307} produced expanded and matured cups (**Figure 3h**). Apparently closed vesicles with diameters of 710 ± 70 nm were observed in cells expressing full-length ATG16L1 (**Figure 3e, i** and **Supplementary Movie 6**). Furthermore, rims of cups were decorated by a striated protein coat that was identical to that seen in reconstitutions in vitro (**Extended Data Figure 6c**). Taken together, ATG16L1 variants stabilized intermediates of membrane cups in reconstitutions on SLBs in vitro and at the PM in cells, providing snapshots of cup formation at distinct stages.

Function of ATG16L1 in starvation-induced autophagy

The formation of membrane cups is a hallmark of nonselective autophagy and our data suggests that this process is driven by ATG16L1. To test this hypothesis, we studied the autophagic activity of ATG16L1 variants that blocked cup formation. We first determined the E3-ligase activity of our different ATG12–ATG5-ATG16L1 complexes. We found that ATG16L1^{NT} and ATG16L1^{207} complexes that lacked the WIPI2 binding site did not promote LC3B conjugation in ATG16L1 KO cells, while ATG16L1^{230}, ATG16L1^{264}, ATG16L1^{307} and ATG16L1^{FL} fully restored lipidation in vivo (**Extended Data Figure 7a**).

Membrane remodeling by ATG16L1 depends on its capacity to bind lipids. We thus compared ATG16L1 levels in cytosolic and membrane fractions of ATG16L1 KO cells that expressed the different ATG16L1 variants. Consistent with in vitro data from a previous study[28], ATG16L1^{307} and ATG16L1^{FL} were enriched in membrane fractions, while membrane binding was strongly impaired for the other variants in which at least a part of the C-terminal lipid binding region was missing (**Extended Data Figure 7b**). A similar difference was observed regarding the intracellular localization of ATG16L1 variants. While ATG16L1^{307} and ATG16L1^{FL} were present at bigger ring-like structures, which might represent matured or complete autophagosomes (**Extended Data Figure 7c, e**), ATG16L1^{230} and ATG16L1^{264} formed much smaller puncta (**Extended Data Figure 7c, d**). To reveal whether these puncta correspond to immature autophagosomes, we compared the flux of autophagic cargo in cells using GFP-RFP-LC3B as a reporter. Consistent with delivery of cargo to lysosomes, a mixture of yellow (cytosolic) and red (lysosomal) LC3B puncta was observed in wildtype cells, while only yellow puncta were observed in ATG16L1 KO cells (**Extended Data Figure 7f**). In wildtype and ATG16L1 KO cells that overexpressed ATG16L1 only yellow puncta that colocalized with ATG16L1 were observed (**Extended Data Figure 7g**), suggesting that autophagosomes are retained in the cytoplasm. The same was true for ATG16L1 KO cells that expressed ATG16L1^{230}, ATG16L1^{264} and ATG16L1^{307}, suggesting that small and big LC3B-positive ATG16L1 puncta correspond to cytoplasmic phagophores and autophagosomes, respectively (**Extended Data Figure 7h**). To identify the nature of these ATG16L1 puncta, we determined their ultrastructure by correlative light electron microscopy (CLEM). Large ATG16L1 puncta in ATG16L1^{FL} and ATG16L1^{307} expressing ATG16L1 KO cells corresponded to complete autophagosomes and vesicular clusters that have recently been reported to contribute to the formation of pre-autophagic structures[31] (**Figure 4a** and **Supplementary Movies 8** and **9**). However, fewer ATG16L1 vesicles were present in ATG16L1^{230} and ATG16L1^{264} expressing cells (**Figure 4b** and **Supplementary Movies 10** and **11**). Moreover, small ATG16L1 puncta colocalized with ER-mitochondrial contact sites (**Figure 4b**) and neither immature nor mature autophagosomes were detected. Taken together, we found a strict correlation between cup-formation in reconstitutions and formation of autophagosomes in cells. ATG16L1 variants that deform membranes into mature cups also promote the formation of autophagosomes, while variants that form premature cups inhibited the formation of autophagosomes.

Discussion

The conjugation of ATG8 proteins to phagophore membranes by an Ub-like conjugation system is a key step during the formation of autophagosomes. LC3B and its E3-ligase complex promote phagophore expansion and the high abundance of LC3B on phagophore membranes made LC3B a widely used marker for autophagosomes in nonselective autophagy[24,32]. Moreover, the E3-ligase complex remains associated with phagophores throughout expansion, but its subunits ATG16L1 and ATG5 are exclusively targeted to their outer membrane[33,34], suggesting that the complex itself exhibit an asymmetric distribution on phagophores. Furthermore, recent studies showed that LC3 proteins are dispensable for selective autophagy[20,21,23] but elongated, unclosed phagophores accumulate in cells lacking

components of the conjugation machinery[35,36]. Although all these data provide plenty of evidence that LC3 proteins are particularly important for phagophore expansion, the following questions remain: what is the molecular function of LC3s in nonselective autophagy, why does the E3-ligase remain associated with phagophores throughout their expansion and why is the localization of the ligase restricted to the outer face of phagophores.

Here, we found that ATG12–ATG5-ATG16L1 not only conjugates LC3B to membranes, but also assembles together with LC3B into membrane coats that cover extensive areas of flat membranes in vitro. Furthermore, LC3B and ATG12–ATG5-ATG16L1 deform flat membranes into cups that share remarkable similarity to phagophores. The highly bent rim of these cups is covered by a dense coat of ATG16L1, suggesting that ATG16L1 stabilizes highly curved membranes. This observation is consistent with a recent mathematical model predicting that phagophore rims need to be stabilized by a protein coat to prevent their premature collapse[37]. This model also predicted that subunits of this rim-coat partitions to the outer face of phagophores during phagophore expansion and rim constriction, which would explain why ATG16L1 is only present at the outer face of phagophores.

The preference of ATG16L1 to bind highly curved membranes is also reflected by its presence on clusters of small vesicles which are involved in autophagy initiation[31]. We observed similar clusters of ATG16L1 vesicles by CLEM and most of these vesicles possessed diameters that were identical to rim-diameters of membrane cups that we observed in our reconstitutions. Much fewer vesicles were observed in cells expressing ATG16L1^{230} (**Extended Data Figure 8a**), arguing that ATG16L1 is involved in the biogenesis of such vesicles. This suggests that ATG16L1 not only senses membrane curvature, but remodels flat membranes into highly curved structures. Accordingly, we found that ATG12–ATG5-ATG16L1 and LC3B deform GUV membranes, remodel SLBs into cup-like structures and induce the formation of membrane cups on omegasome-like membranes in cells, but no such membrane deformations were observed in the absence of ATG16L1. Interestingly, ATG16L1^{230} and ATG16L1^{264}, which lack a part of the C-terminal membrane binding region, were impaired in cup formation but deformed flat membranes into highly bent rims, suggesting that the C-terminal membrane binding region is required for cup formation, but dispensable for membrane bending.

Interestingly, intermediate structures such as premature membrane cups that we observed on omegasome-like membranes in cells expressing ATG16L1^{FL} correspond to endpoints of cup formation in cells expressing ATG16L1^{230}, ATG16L1^{264} and ATG16L1^{307} (**Figure 4c**). This suggests that ATG16L1 variants stall cup-formation at distinct stages. Moreover, the capacity of ATG16L1 variants to deform membranes into cups correlates with their ability to promote the formation of autophagosomes in starved cells. Apparently completed autophagosomes were only observed in cells expressing ATG16L1^{307} and ATG16L1^{FL}, which also supported the formation of fully expanded membrane cups on SLBs in vitro and on phagophore-like membranes in vivo. By contrast, ATG16L1^{230} and ATG16L1^{264} failed to induce the formation of autophagosomes in vivo. Instead, both variants colocalized mostly with ER-mitochondria contact sites which serve as sites of phagophore formation[38], suggesting that they stall

phagophore formation at an early stage. Accordingly, rim-like structure or premature cups were observed on SLBs in in vitro reconstitutions and on omegasome-like membranes in cells expressing ATG16L1^{230} or ATG16L1^{264}.

Based on our observations and on predictions from mathematical modelling of phagophore formation[37], we propose that autophagy starts with the assembly of a circular ATG16L1 coat that buckles the membrane into a highly bent rim (inset 1 and 2 in **Extended Data Figure 8b**, **Figure 4d** and **Supplementary Movie 12**). Removal of ATG16L1 subunits from the rim coat leads to a constriction of these rings which deforms membranes into cups. Partitioning of ATG16L1 to the outer face further stabilizes membrane cups, which explains the asymmetric distribution of ATG16L1 on phagophores[34]. Consistent with this model, membrane cups that we observed at omegasome-like membranes in WIPI2-CAAX expressing cells were decorated with LC3B and ATG16L1 (**Extended Data Figure 5g**). The evolution of these cups into mature vesicles (insets 3-6 in **Extended Data Figure 8b**) requires stabilization of shallow membrane curvatures at a mesoscopic scale which could be supported by membrane coats that we observed on SLBs in vitro. Our model also consistent with the observation that LC3B is dispensable for selective but important for nonselective autophagy. In selective autophagy, cargo defines the size and shape of phagophores. The formation of pre-shaped cups would thus be counterproductive. The opposite is true for nonselective autophagy, in which free standing membrane cups ensure that bulk cytoplasm can be sequestered.

In summary, we demonstrated that ATG16L1 is an unconventional membrane remodeling protein that cooperates with LC3B to generate phagophore-like membrane cups. We thus propose that nonselective phagophores are generated by ATG16L1 driven remodeling of omegasomes.

Methods

Details regarding the used reagents, antibodies and primers are summarized in Supplementary Table 2.

Protein purification

Human ATG proteins were expressed as fusion proteins with N-terminal affinity tags as indicated in Supplementary Table 2. LC3B was expressed as processed, conjugation-competent variant lacking its C-terminal propeptide (referred to as LC3B^{G120}). ATG12-ATG5 was expressed using a polycistronic vector harboring cDNAs of *ATG7*, *ATG10*, *ATG5* and His10-tagged *ATG12*. LC3B, ATG3, ATG12–ATG5 and ATG16L1 variants were produced in E.coli. Cells were grown at 37°C, 180 rpm until the OD_{600} reached 0.6. Expression was induced by adding 0.3 mM IPTG and cells were grown further for 3 h at 37°C or at 18°C overnight (ATG16 variants). *E. coli* cells were harvested by centrifugation at 4500 g for 10 minutes, resuspended in lysis buffer (100 mM Tris-HCl pH 8.0, 300 mM NaCl (500 mM for ATG16L1), 20 mM imidazole, 10 % glycerol, 5 mM beta-mercaptoethanol) supplemented with complete protease inhibitor

cocktail (Sigma) and benzonase (Sigma). Cells were lysed using an Avestin Emulsiflex C3 (ATA Scientific).

ATG7 and ATG16L1^{FL} (full-length) were expressed in SF9 and Hi5 cells, respectively, and grown to 1x10^6 cells/ml in EX-CELL 420 serum-free medium supplemented with 5 % Fetal Bovine Serum for SF9 cells. Baculovirus-infected insect cells were added in a ratio of 1:4000 (ATG7) and 1:1000 (ATG16L1). Cultures were incubated for 72 h at 25°C and 90 rpm. Cells were harvested by centrifugation at 2000 g for 15 minutes, washed with Dulbecco's phosphate buffered saline (DPBS, Gibco), resuspended in lysis buffer (without beta-mercaptoethanol for ATG7) and lysed using a dounce homogenizer. Soluble fractions of all cell lysates were collected after centrifugation at 45000 g for 1 h and incubated with Ni-NTA agarose for 1 h at 4°C. Unbound proteins were removed by washing with wash buffer (50 mM Tris-HCl pH 8.0, 300 mM NaCl (500 mM for ATG16L1), 5 mM imidazole, 10 % glycerol, 5 mM beta-mercaptoethanol) and eluted using elution buffer (50 mM Tris-HCl pH 7.4, 300 mM NaCl (500 mM for ATG16L1), 500 mM imidazole, 10 % glycerol). Except for ATG16L1$^{11-43}$, the affinity tags were removed by Prescission protease treatment for 45 min at room temperature in presence of 5 mM DTT (AppliChem) and 1 mM EDTA (Carl Roth). The His-MBP tag of ATG16L1$^{11-43}$ was cleaved by Prescission protease treatment in presence of ATG12-ATG5. The digested proteins were subjected to size exclusion chromatography on HiLoad 16/60 Superdex 75 (ATG3 and LC3B) or Superdex 200 (ATG12-ATG5, ATG7, ATG16L1 and -variants) columns, equilibrated with SEC buffer (25 mM Tris-HCl pH 7.4, 275 mM NaCl or 400 mM for ATG16L1) using an ÄKTA explorer (GE healthcare). The elution fractions containing protein of interest were pooled, concentrated and aliquots were flash frozen in liquid nitrogen and stored at -80°C. Protein quality and integrity of the ATG12-ATG5-ATG16L1$^{11-43}$ complex were characterized by SDS-PAGE and mass spectrometry.

Fluorescent labelling of proteins

Fluorescent labeling of proteins was performed using maleimide-coupling chemistry. Alexa Fluor 488 C_5 (Molecular Probes) was conjugated to an introduced N-terminal cysteine of LC3B while Atto590 (ATTO-TEC) was conjugated to native cysteine residues in ATG16L1. Purified proteins were incubated with an equimolar amount of fluorescent dyes for 1 h at room-temperature. Unbound dyes were removed by using HiTrap Desalting columns (GE healthcare, for LC3B), or Zeba Spin Desalting Columns (Thermo scientific, for ATG16L1). Labelling efficiency was determined spectroscopically.

Model membranes

Giant Unilamellar Vesicles (GUVs) were generated by electroformation on indium-tin oxide coated glass slides in custom made Teflon chambers[39]. The lipid mixture consisting of 1,2-dioleoyl-sn-glycero-3-phosphoethanolamine (DOPE, 18:1 PE, 39.9 mol%), 1,2-dioleoyl-sn-glycero-3-phosphocholine (DOPC, 18:1 PC, 40 mol%), 1-palmitoyl-2-oleoyl-sn-glycero-L-serine (POPS, 16:0-18:1 PS, 10 mol%), cholesterol (10

mol%) and lissamine rhodamine PE (0.1 mol%) was deposited on slides and dried in vacuum for 60 minutes. The two glass plates were placed face-to-face in the assembled chamber by maintaining a 2 mm gap between them. The chamber was filled with 600 mOsM sucrose solution an alternating electric current (2 V, 10 Hz) was applied for 4 h. GUVs were diluted 1:1 with 600 mOsM sucrose solution and used immediately.

Supported lipid bilayers (SLB) were produced from a suspension of small unilamellar vesicles (SUVs), which were generated by hydration of a thin vacuum dried lipid film (same composition as for GUV production) using liposome buffer (12.5 mM Tris HCl pH 7.4, 137.5 mM NaCl, 0.1 mM DTT and 1 mM ATP/Mg^{2+}). The suspension was subjected to 3-5 freeze-thawing cycles followed by sonication for 30 min. The size of liposomes was measured by dynamic light scattering. 200 µl of SUV suspension was supplemented with 1 mM $CaCl_2$ and deposited either on freshly generated silanized mica or plasma cleaned glass coverslips and incubated at room temperature for 30 min. Unbound vesicles were removed by washing with SEC buffer.

Reconstitution of LC3B conjugation reaction

LC3B was preincubated with ATP/Mg^{2+}, DTT, ATG7 and ATG3 at 37°C for 30 min before reconstituted ATG12–ATG5-ATG16L1 (variant) complexes were added. 100 µL of the mixture was added to 100 µL of GUV suspension in IBIDI chambers to reach final concentrations of 1 mM ATP/Mg^{2+}, 0.1 mM DTT, 1 µM ATG7, 1.5 µM ATG3, 6 µM LC3B (2:1 ratio of unlabeled to labelled) and 1 µM ATG12-ATG5-ATG16L1, and incubated for 1 h at 37°C. The conjugation of LC3B to SLBs was carried out as described for GUVs using AFM chambers and unbound protein was removed by extensive washing with SEC buffer.

Confocal Microscopy

Confocal images of GUVs and fixed cells were acquired on a Leica TCS SP8 AOBS Confocal Laser Scanning Microscope (×63/1.4 NA objective) using the Leica LAS AF SP8 software. Atto405, GFP/$Alexa^{488}$, rhodamine/mCherry/RFP/$Alexa^{561}$, and $Alexa^{633}$ dyes were excited with 405 nm, 488 nm, 561 nm and 633 nm laser light, respectively. Multi-tracking was used for image acquisition and pinholes were set for acquisition of 0.5-1.0 µm optical slices. Images were analyzed using Fiji.

Fluorescence Recovery after Photobleaching

FRAP experiments were performed using a Leica-TCS-SP8 microscope. The images were acquired using a 63x objective with a resolution of 512 x 512 pixel and a pinhole set to 1.0 µm. Fluorescence corresponding to 10 % of the total GUV area or of indicated SLB areas was bleached using 100 % laser power. Fluorescence recovery was observed by recording 104 frames over 6-8 min. Images were analyzed using Fiji using a non-bleached part of the same GUV to correct for bleaching during recovery and

background fluorescence. FRAP curves were fitted to the exponential decay function y = a (1 − e (−xb)) with mobile fractions = a and half-times t1/2 = −log (0.5)/b.

Atomic Force Microscopy

The atomic force microscopy was performed on a BRUKER ScanAsyst. Peak force tapping mode AFM images were acquired using SCANASYST-FLUID cantilevers (BRUKER). The peak force oscillation frequency was set to 150 kHZ and the set point was assigned to 200 pN. Resolution of images were 512 x 512 pixels.

Cell culture

HeLa cells were purchased from Cell Lines Service (# 300194) and cultured in DMEM (Gibco, 31966-021) containing 10 % FBS (Sigma-Aldrich, F4135), 100 U/ml penicillin and 100 µM streptomycin (Gibco, 15140-122) at 37^{o}C in a 5 % CO_2 atmosphere. Starvation of HeLa cells was induced by washing them three times with DPBS and incubation for 2 h in presence of Earle's Balanced Salt Solution (EBSS, Sigma Aldrich, E2888). HeLa cells were transfected with TransIT-HeLaMONSTER Transfection Kit (Mirus, MIR2904)) or using JetPRIME ® (Polyplus 114-01) as per manufacturer's protocol and analyzed 24 h to 48 h post-transfection.

Cloning

Plasmids and primers are listed in Supplementary Table 2. The cDNA clones coding for ATG7 (isoform 1), ATG3, ATG12, ATG5, ATG16L1 and LC3B were cloned as described previously[18]. HA-tagged ATG16L1 was generated by cloning a 3x HA-tag and the cDNA of ATG16L1, separated by a linker (AQCS $(GA)_6$GPTENSS), into pLPCX (Clontech) between *Hind*III and *Not*I restriction sites. ATG16L1 truncations were amplified by PCR using the full-length construct as template and cloned into the pLPCX vector using the same restriction sites. RFP-GFP-LC3B was generated by inserting the cDNA of LC3B into pTfLC3 (Addgene plasmid #21074) using *Bgl*II and *Kpn*I restriction sites. Cloning of the GFP-LC3B construct and generation of CRISPR-Cas9 ATG16 knock out cells was described previously[18] and WIPI2b-CAAX construct was a gift from Sharon Tooze[17]. ATG14 cDNA from pEGFP-ATG14L (Addgene plasmid # 21635) was inserted into pmKate2-C1 (Euromedex EV-FP181) using the compatible restriction sites EcoRI and KpnI. Site-directed mutagenesis was used to restore the reading frame by inserting an adenine at position 1331.

LC3B lipidation assay

ATG16L1 knock out HeLa cells were rescued by transfecting N-terminal HA tagged ATG16 variants or full-length ATG16L1 as indicated for 24 h. Cells were washed with PBS and starved for 2 h in EBSS. The cells

were harvested following trypsination and lysed with lysis buffer (150 mM NaCl, 1 % NP-40, 50 mM Tris pH 7.4) supplemented with 1 mM PMSF (Roth) and complete protease inhibitor cocktail (Sigma Aldrich; Roche) for 30 min on ice. The cell lysate was centrifuged at 10000 g for 10 min. The protein concentration of the supernatant was measured by Pierce BCA protein assay kit (Thermo Fischer). Equal amounts of cell lysate mixed with 5x sample buffer was subjected to NUPAGE 4-12 % Bis-Tris Gel (Invitrogen), transferred to PVDF membrane and blotted with specific primary antibody and HRP-conjugated secondary antibodies. Membrane was thoroughly washed 3 times and developed with Super signal West Pico chemiluminescent substrate (Thermo Fischer). Detection was performed by a GelDoc documentation system and analysis by ImageJ.

Cytosol and membrane fraction (Cell fractionation)

Membrane fractions were prepared as previously reported[28]. Cells were harvested by centrifugation at 1500 g for 10 min and the pellet was dissolved in fractionation buffer (20 mM HEPES-KOH pH 7.4, 100 mM potassium acetate, 85 mM sucrose, 1 mM magnesium acetate supplemented with 1 mM PMSF and complete protease inhibitor cocktail). Cell lysis was performed by applying three freeze-thawing cycles and cell lysate was centrifuged at 1500 g for 5 min. The soluble cytoplasmic fraction was prepared by centrifugation of the supernatant at 70000 g for 30 min. The pellets from both the spins were dissolved in fractionation buffer containing 1 % NP-40 and centrifuged at 70000 g for 30 min. The supernatant from the second high speed run corresponds to the membrane fraction and was together with the cytosolic fractions analyzed by western blotting.

Starvation-dependent recruitment of LC3B to the PM

Cells plated onto IBIDI µ-well dishes were transfected with 65 % WIPI2-CAAX, 25 % ATG16L1 and 20 % GFP-LC3B using Mirus Hela Monster kit (Mirus 2904) according to manufacturer's instructions. Two days post-transfection, cells were washed with PBS and incubated with EBSS starvation medium for indicated times at 37°C in a 5% CO_2 atmosphere. Cells were imaged immediately after starvation. Ten non-overlapping fields of view were analysed and Z-stacks covering the entire cell volume were recorded for each condition. The number of cells in which LC3B was targeted to the plasma membrane was assessed in each field of view and expressed as percentage of total number of transfected cells.

Autophagy inhibition

HeLa cells were transfected with 65 % WIPI2-CAAX, 25 % ATG16L1 and 20 % GFP-LC3B using the Mirus HeLa Monster kit, according to manufacturer's instructions. At 48 h post-transfection, cells were treated with 0.5 µM SAR405 (Ape Bio A8883) for 8 h (or untreated control) followed by starvation for 2 h in EBSS (or fed in full DMEM). Alternatively, cells were incubated with 10 µM SBI-0206965 (Sigma Aldrich,

SML1540; or untreated, control) and starved for 2 h in EBSS medium (or fed in full DMEM). Cells were fixed for 10 min at room temperature in 4% PFA in PBS and mounted onto glass slides.

Quantification of LC3B and ATG16L1 puncta

Z-stacks were converted into maximum projections using Fiji and LC3B puncta were counted using the Particle Analysis Plugin. For each projection, a threshold was manually set to identify particles of interest. The particles were analysed using a size range from 0.2 to 1 µm and a circularity between 0 to 1. The number of puncta per cell was assessed in 10 randomly chosen fields of view per condition. The same procedure was used to count ATG16L1 puncta, but the size range was set to 0.1-0.7 µm and 0.7-2.0 µm, respectively.

siRNA treatment

Semiconfluent HeLa cells were transfected with control (scrambled), ATG14 or ULK1 siRNA. All siRNA treatments were performed in serum- and antibiotic-free culture medium, using JetPRIME® (Polyplus 114-01) according to manufacturer's instructions. After 24 h, the medium was replaced by fresh full DMEM and DNA transfection (60 % WIPI2-CAAX, 25 % ATG16L1 and 25 % GFP-LC3B) was carried out using *Trans*IT-HeLa MONSTER (Mirus 2904) and incubated 24 h. Cells were washed with PBS and analysed by immunofluorescence and western blot.

Cell unroofing and immunogold labeling

Unroofing was performed by sonication as previously described[15]. Coverslips where quickly rinsed three times in Ringer+Ca (155 mM NaCl, 3 mM KCl, 3 mM NaH_2PO_4, 5 mM HEPES, 10 mM glucose, 2 mM $CaCl_2$, 1 mM $MgCl_2$, pH 7.2), then immersed 10 s in Ringer-Ca (155 mM NaCl, 3 mM KCl, 3 mM NaH_2PO_4, 5 mM HEPES, 10 mM glucose, 3 mM EGTA, 5 mM $MgCl_2$, pH 7.2) containing 0.5 mg/mL poly-L-lysine) and quickly rinsed in Ringer-Ca. Cells were unroofed by scanning the coverslip with rapid (2-5 s) sonicator pulses at the lowest deliverable power in KHMgE buffer (70 mM KCl, 30 mM HEPES, 5 mM $MgCl_2$, 3 mM EGTA, pH 7.2).

Unroofed cells were immediately fixed using fixative in KHMgE: 4 % PFA for 45 min for PREM of immunogold-labeled samples, 3 % PFA and 1 % glutaraldehyde or 2 % PFA and 2 % glutaraldehyde for 10 to 20 min for PREM. Glutaraldehyde-fixed samples were subsequently quenched using 0.1% $NaBH_4$ in KHMgE for 10 minutes. Immunogold labeling was performed in detergent-free buffer (KHMgE, 1 % BSA), samples were blocked for 30 min, incubated 1 h and 30 min with the primary antibody (using a 1:20 dilution), rinsed and incubated two times 20 min with the gold-coupled secondary antibodies. Samples were rinsed again and post-fixed with 2% glutaraldehyde.

Platinum-replica sample processing

Cells and SLBs were further sequentially treated with 0.5 % OsO_4, 1 % tannic acid and 1 % uranyl acetate prior to graded ethanol dehydration and hexamethyldisilazane substitution (HMDS) (Sigma). Dried samples were then rotary-shadowed with 2 nm of platinum and 5-8 nm of carbon using an ACE600 high vacuum metal coater (Leica Microsystems). The resultant platinum replicas were floated off the glass with hydrofluoric acid (5 %), washed several times on distilled water, and picked up on 200 mesh formvar/carbon-coated EM grids.

EM of platinum replicas

Replicas on EM grids were mounted in a eucentric side-entry goniometer stage of a transmission electron microscope operated at 80 kV (model CM120; Philips) and images were recorded with a Morada digital camera (Olympus). Images were processed in Photoshop (Adobe) to adjust brightness and contrast and presented in inverted contrast. Tomograms were made by collecting images at the tilt angles up to ± 25° relative to the plane of the sample with 5° increments. Images were aligned by layering them on top of each other in Photoshop. Measurements of cup length and width were performed on high magnification PREM views using ImageJ.

Thin-section Transmission Electron Microscopy

Cells were fixed with 4 % paraformaldehyde and 0.2 % glutaraldehyde for 10 min followed by 2 % paraformaldehyde and 0.1 % glutaraldehyde for two hours at RT. Cells were washed with PBS and 1% gelatin in PBS was added before cells were collected, pelleted (5000 g, 5 min) and resuspended in 10% gelatin (5 min at 37°C). Cells were again collected (8000 g, 5 min), the pellet was cut into blocks and incubated in 2.3 M sucrose solution at 4°C overnight. Blocks were frozen in liquid nitrogen and 150 nm ultrathin sections were prepared using a Leica-UC6-FC6 ultramicrotome equipped with a Leica 16DIA.DCIMM3530 diamond knife at -120 °C with a speed of 0.8 mm/s. Ribbons were mounted on carbon-coated copper finder grids (Oxford instruments AGG245) and tomograms were recorded using a Tecnai Biotwin 120 electron microscope at magnification of 23,000x with a tilt range from 50° to -50° and 5° increments. Tilt series were aligned and reconstructed using the IMOD software package and further processed with Amira 2019.3 (Thermo Fisher Scientific).

Statistics and reproducibility

Quantifications were performed from at least three (two for cell fractionation) independent experiments or from at least 20 cells and values are expressed as mean ± standard deviation. All parameters including significance and n-values are specified in each figure legend. Statistical significance between two independent samples was determined using a two tailed unpaired t-test. P values of < 0.05 were

considered statistically significant and significance levels were indicated by *P< 0.05; **P< 0.01; ***P< 0.001. The corresponding charts were generated by Excel or Prism – GraphPad software.

Data availability

Source data for figures and numbers, including quantifications shown in charts and full blots of display items in figures are available in Supplementary Table 1 and Supplementary Figure in the Supplementary Material. The authors declare that all data supporting the findings of this study are available in the paper and its supplementary material.

Declarations

Acknowledgements

We thank Frank Lafont and Sebastien Janel (Center for Infection and Immunity of Lille, Institut Pasteur de Lille, Lille, France) for access to atomic force microscopes, scientific and technical support and fruitful discussions. We thank Alexis Canette (Institut de Biologie Paris-Seine (IBPS) Electron Microscopy facility) for help with metal coaters. We also thank Sharon Tooze (The Francis Crick Institute, London, UK) for the WIPI2-CAAX construct and fruitful discussions. We thank Anastasia Gazi, Olivier Gorgette and Gérard Pehau-Arnaudet of the Ultrastructural BioImaging Platform (UTechS UBI, Institut Pasteur Paris) for access to electron microscopy and sample preparation equipment as well as for technical support and training. We thank Jacomina Krijnse Locker (Paul-Ehrlich-Institut and formerly at the Institut Pasteur Paris) for helpful discussions and support. We thank Arnaud Echard and Chiara Zurzolo (Institut Pasteur, Paris) for commenting on the manuscript.

Funding

This work was supported by the ERC-Starting Grant GA 638603 (Autophagy in vitro) to TW and by Sorbonne Université, INSERM, Association Institut de Myologie core funding and the Agence Nationale de la Recherche (grant ANR14-CE12-0001-01) to SV.

Author contribution

Conceptualization: TW; Methodology: TW, SV; Investigation: JM, CG-B, SM, CN, SR, SV, TW; Visualization: JM, CG-B, SM, CN, SR, SV, TW; Funding acquisition: SV and TW; Project administration: TW;

Supervision: TW; Writing – original draft: TW; Writing – review & editing: TW, SV, JM,CN

Competing interests

Authors declare that they have no competing interests.

Additional Information

Supplementary Information is available for this paper.

Correspondence and requests for material should be sent to thomas.wollert@pasteur.fr and s.vassilopoulos@institut-myologie.org.

Reprints and permissions information is available at www.nature.com/reprints.

References

1. Galluzzi, L. *et al.* Molecular definitions of autophagy and related processes. *Embo J* **36**, 1811–1836 (2017).

2. Kirkin, V. & Rogov, V. V. A Diversity of Selective Autophagy Receptors Determines the Specificity of the Autophagy Pathway. *Mol Cell* **76**, 268–285 (2019).

3. González, A. & Hall, M. N. Nutrient sensing and TOR signaling in yeast and mammals. *Embo J* **36**, 397–408 (2017).

4. Johansen, T. & Lamark, T. Selective Autophagy: ATG8 Family Proteins, LIR Motifs and Cargo Receptors. *J Mol Biol* **432**, 80–103 (2019).

5. Eickhorst, C., Licheva, M. & Kraft, C. Scaffold proteins in bulk and selective autophagy. *Prog Mol Biol Transl* **172**, 15–35 (2020).

6. Orsi, A. *et al.* Dynamic and transient interactions of Atg9 with autophagosomes, but not membrane integration, are required for autophagy. *Mol Biol Cell* **23**, 1860–1873 (2012).

7. Tito, S. D., Hervás, J. H., Vliet, A. R. van & Tooze, S. A. The Golgi as an Assembly Line to the Autophagosome. *Trends Biochem Sci* **45**, 484–496 (2020).

8. Ge, L., Melville, D., Zhang, M. & Schekman, R. The ER-Golgi intermediate compartment is a key membrane source for the LC3 lipidation step of autophagosome biogenesis. *eLife* **2013**, e00947 (2013).

9. Ravikumar, B., Moreau, K., Jahreiss, L., Puri, C. & Rubinsztein, D. C. Plasma membrane contributes to the formation of pre-autophagosomal structures. *Nat Cell Biol* **12**, 747–757 (2010).

10. Hailey, D. W. *et al.* Mitochondria Supply Membranes for Autophagosome Biogenesis during Starvation. *Cell* **141**, 656–667 (2010).

11. Dupont, N. *et al.* Neutral Lipid Stores and Lipase PNPLA5 Contribute to Autophagosome Biogenesis. *Curr Biol* **24**, 609–620 (2014).

12. Maeda, S., Otomo, C. & Otomo, T. The autophagic membrane tether ATG2A transfers lipids between membranes. *Elife* **8**, e45777 (2019).

13. Mizushima, N. The ATG conjugation systems in autophagy. *Curr Opin Cell Biol* **63**, 1–10 (2020).

14. Tanida, I., Tanida-Miyake, E., Komatsu, M., Ueno, T. & Kominami, E. Human Apg3p/Aut1p Homologue Is an Authentic E2 Enzyme for Multiple Substrates, GATE-16, GABARAP, and MAP-LC3, and Facilitates the Conjugation of hApg12p to hApg5p*. *J Biol Chem* **277**, 13739–13744 (2002).

15. Sou, Y. *et al.* The Atg8 Conjugation System Is Indispensable for Proper Development of Autophagic Isolation Membranes in Mice. *Mol Biol Cell* **19**, 4762–4775 (2008).

16. Tanida, I. *et al.* HsAtg4B/HsApg4B/Autophagin-1 Cleaves the Carboxyl Termini of Three Human Atg8 Homologues and Delipidates Microtubule-associated Protein Light Chain 3- and GABAA Receptor-associated Protein-Phospholipid Conjugates*. *J Biol Chem* **279**, 36268–36276 (2004).

17. Dooley, H. C. *et al.* WIPI2 Links LC3 Conjugation with PI3P, Autophagosome Formation, and Pathogen Clearance by Recruiting Atg12–5-16L1. *Mol Cell* **55**, 238–252 (2014).

18. Wetzel, L. *et al.* TECPR1 promotes aggrephagy by direct recruitment of LC3C autophagosomes to lysosomes. *Nat Commun* **11**, 2993 (2020).

19. Chen, D. *et al.* A Mammalian Autophagosome Maturation Mechanism Mediated by TECPR1 and the Atg12-Atg5 Conjugate. *Mol Cell* **45**, 629–641 (2012).

20. Nguyen, T. N. *et al.* Atg8 family LC3/GABARAP proteins are crucial for autophagosome–lysosome fusion but not autophagosome formation during PINK1/Parkin mitophagy and starvation. *J Cell Biol* **215**, 857–874 (2016).

21. Nguyen, T. N. *et al.* ATG4 family proteins drive phagophore growth independently of the LC3/GABARAP lipidation system. *Mol Cell* **81**, 2013-2030.e9 (2021).

22. Vaites, L. P., Paulo, J. A., Huttlin, E. L. & Harper, J. W. Systematic analysis of human cells lacking ATG8 proteins uncovers roles for GABARAPs and the CCZ1/MON1 regulator C18orf8/RMC1 in macro and selective autophagic flux. *Mol Cell Biol* **38**, e00392-17 (2017).

23. Tsuboyama, K. *et al.* The ATG conjugation systems are important for degradation of the inner autophagosomal membrane. *Science* **354**, 1036–1041 (2016).

24. Kabeya, Y. *et al.* LC3, a mammalian homologue of yeast Apg8p, is localized in autophagosome membranes after processing. *Embo J* **19**, 5720–5728 (2000).

25. Otomo, C., Metlagel, Z., Takaesu, G. & Otomo, T. Structure of the human ATG12~ATG5 conjugate required for LC3 lipidation in autophagy. *Nat Struct Mol Biol* **20**, 59–66 (2013).

26. Kaufmann, A., Beier, V., Franquelim, H. G. & Wollert, T. Molecular Mechanism of Autophagic Membrane-Scaffold Assembly and Disassembly. *Cell* **156**, 469–481 (2014).

27. Fletcher, K. *et al.* The WD40 domain of ATG16L1 is required for its non-canonical role in lipidation of LC3 at single membranes. *Embo J* **37**, (2018).

28. Lystad, A. H. *et al.* Distinct functions of ATG16L1 isoforms in membrane binding and LC3B lipidation in autophagy-related processes. *Nat Cell Biol* **117**, 2805 (2019).

29. Archna, A. & Scrima, A. Identification, biochemical characterization and crystallization of the central region of human ATG16L1. *Acta Crystallogr Sect F Struct Biology Commun* **73**, 560–567 (2017).

30. Hayashi-Nishino, M. *et al.* A subdomain of the endoplasmic reticulum forms a cradle for autophagosome formation. *Nat Cell Biol* **11**, 1433–1437 (2009).

31. Kumar, S. *et al.* Mammalian hybrid pre-autophagosomal structure HyPAS generates autophagosomes. *Cell* (2021) doi:10.1016/j.cell.2021.10.017.

32. Kimura, S., Noda, T. & Yoshimori, T. Dissection of the Autophagosome Maturation Process by a Novel Reporter Protein, Tandem Fluorescent-Tagged LC3. *Autophagy* **3**, 452–460 (2007).

33. Mizushima, N. *et al.* Dissection of Autophagosome Formation Using Apg5-Deficient Mouse Embryonic Stem Cells. *J Cell Biology* **152**, 657–668 (2001).

34. Mizushima, N. *et al.* Mouse Apg16L, a novel WD-repeat protein, targets to the autophagic isolation membrane with the Apg12-Apg5 conjugate. *J Cell Sci* **116**, 1679–1688 (2003).

35. Kishi-Itakura, C., Koyama-Honda, I., Itakura, E. & Mizushima, N. Ultrastructural analysis of autophagosome organization using mammalian autophagy-deficient cells. *J Cell Sci* **127**, 4089–4102 (2014).

36. Uemura, T. *et al.* A Cluster of Thin Tubular Structures Mediates Transformation of the Endoplasmic Reticulum to Autophagic Isolation Membrane. *Mol Cell Biol* **34**, 1695–1706 (2014).

37. Sakai, Y., Koyama-Honda, I., Tachikawa, M., Knorr, R. L. & Mizushima, N. Modeling Membrane Morphological Change during Autophagosome Formation. *Iscience* **23**, 101466 (2020).

38. Hamasaki, M. *et al.* Autophagosomes form at ER-mitochondria contact sites. *Nature* **495**, 389 393 (2013).

39. Angelova, M. I. & Dimitrov, D. S. Liposome electroformation. *Faraday Discuss Chem Soc* **81**, 303–311 (1986).

Figures

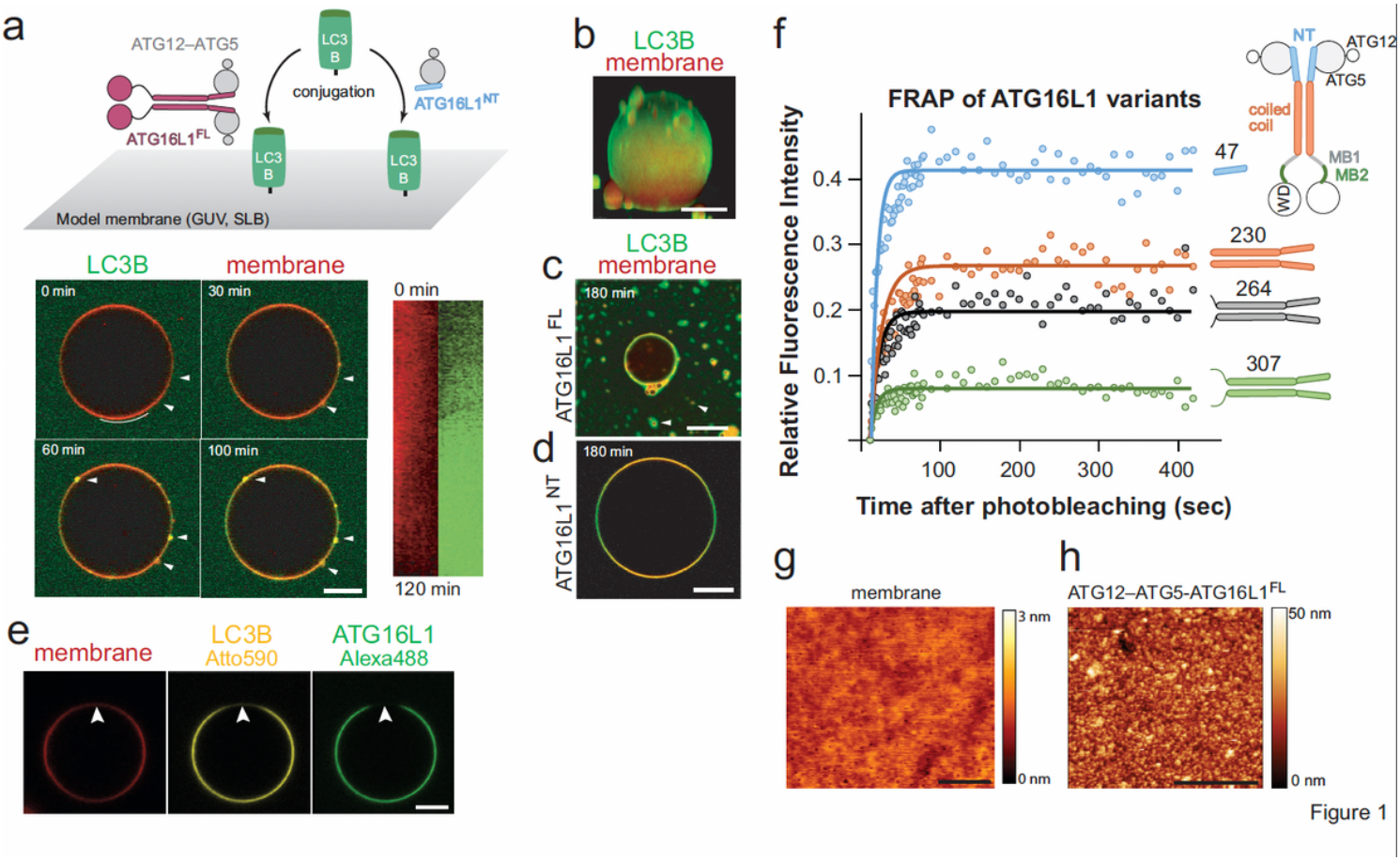

Figure 1

Scaffold formation of LC3B and ATG12–ATG5-ATG16L1 on membranes in vitro.

(**a-d**) Alexa 488 labeled LC3B^{G120} was conjugated to fluorescent labeled Giant Unilamellar Vesicles (GUVs, red) in the presence of unlabeled ATG16L1^{FL} (**a-c**) or ATG16L1^{NT} (**d**) as illustrated by the cartoon. Images show conjugation at indicated timepoints. Arrowheads in (**a**) indicate membrane deformation and kymographs of the area depicted by the white line are shown, (**b**) 3D reconstruction of a GUV after conjugation from a z-stack (see also **Extended Data Figure 1c**), (**e**) FRAP experiment of a GUV (red) to which LC3B$^{G120,\ Atto590}$ was conjugated in the presence of ATG16L1^{Alexa488}. The fluorescence was bleached in the indicated area (arrowhead) and recovery is shown seven minutes after bleaching. Scale bars = 10µm. (**f**) Quantification of FRAP experiments (shown in **Extended Data Figure 2d**) of ATG16L1 variants as indicated. The solid line shows the exponential fit of experimental data (dots). (**g**) AFM height profile (with colors defined in corresponding scales) of a supported lipid bilayer on plasma cleaned glass. (**h**) Similar height profiles after LC3B^{G120} conjugation with ATG16L1. Scale bars = 500 nm. See also

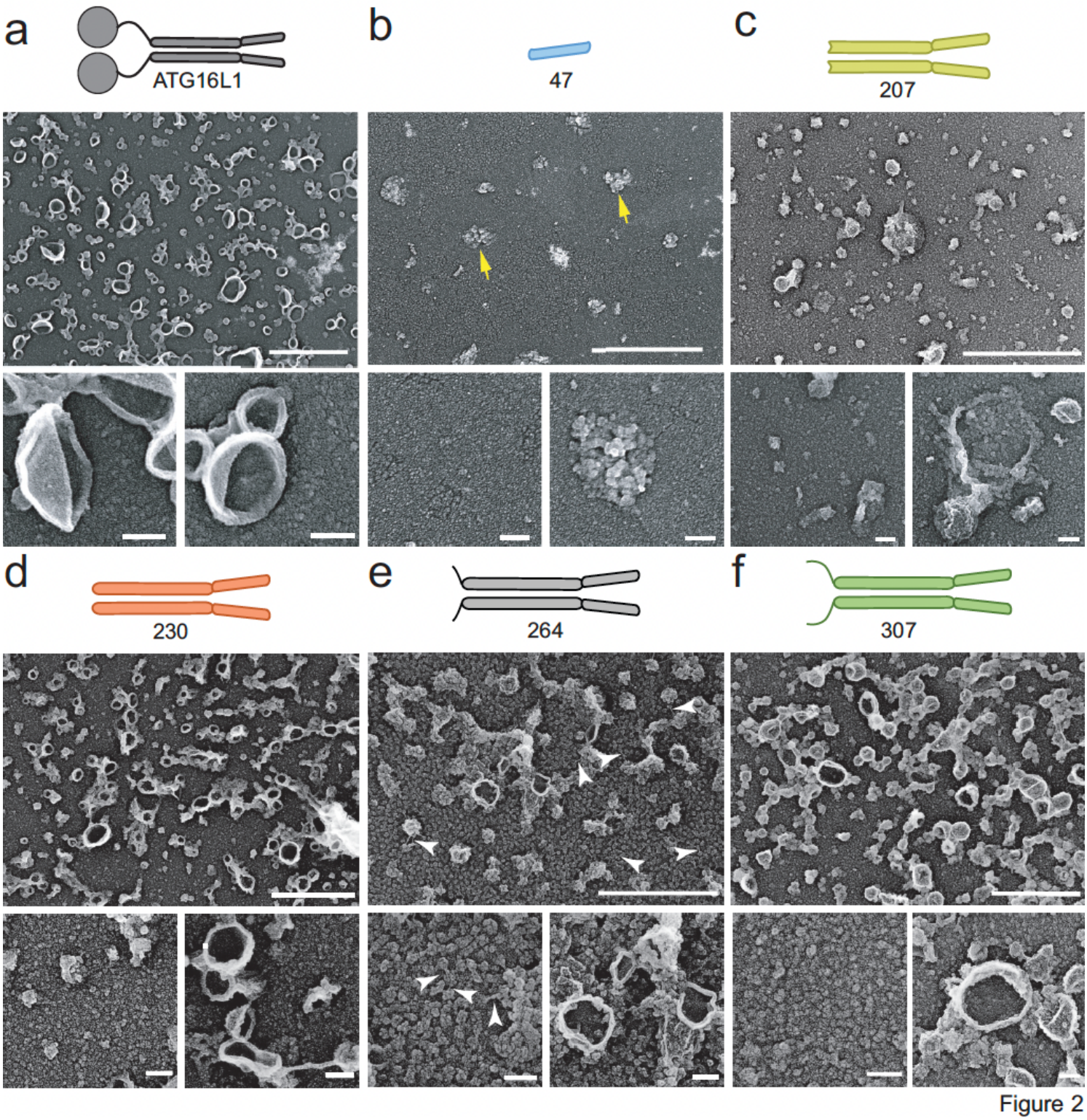

Figure 2

Figure 2

Cup formation by ATG16L1 on SLBs in vitro.

(a-f) High magnification PREM views of SLB to which LC3B was conjugated in the presence of ATG16L1^{FL} (**a**), ATG16L1^{Nt} (**b**), ATG16L1^{207} (**c**), ATG16L1^{230} (**d**), ATG16L1^{264} (**e**) and ATG16L1^{307} (**f**). Scale bars = 1 µm (overview, top panels - general appearance of SLBs), and 100 nm (left panels - insets

focus on protein coats), 100 nm insets (right panels - showing characteristic membrane deformations). Yellow arrows indicate protein aggregates in (**b**) and white arrowheads point rods connecting particles in (**e**), see also **Extended Data Figure 3c**.

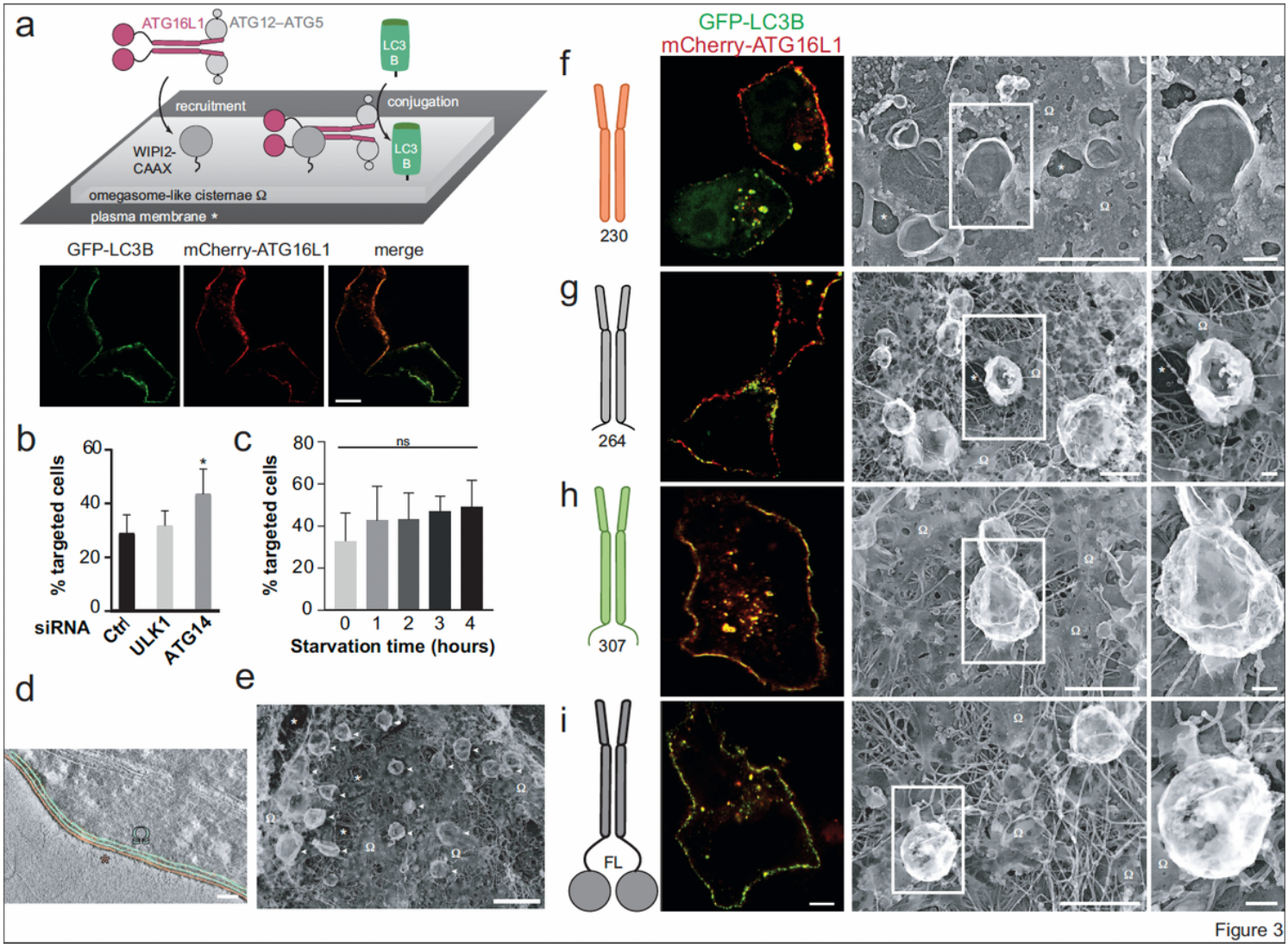

Figure 3

Figure 3

Generation of membrane cups by LC3B and ATG12–ATG5-ATG16L1 in vivo.

(**a**) Confocal image of HeLa cells coexpressing WIPI2-CAAX, GFP-LC3B and mCherry-ATG16L1. Scale bar = 10 µm. (**b**, **c**) Targeting of LC3B to the PM in HeLa cells expressing GFP-LC3B, WIPI2-CAAX and ATG16L1. Data show the percentage of cells with LC3B at the plasma membrane, expressed as mean ± S.D. of N = 5 (**b**) and N = 3 (**c**) independent experiments. (**b**) Cells were treated with scrambled siRNAs (control) or siRNA against ULK1 or ATG14, n_{Ctrl} = 477 cells; n_{ULK1} = 486 cells; n_{ATG14} = 612 cells. Significance from Student's t-test with *p = 0.0308. (**c**) Cells were starved for indicated times, $n_{(0h)}$ = 312 cells, $n_{(1h)}$ = 288 cells, $n_{(2h)}$ = 299 cells, $n_{(3h)}$ = 239 cells and $n_{(4h)}$ = 281 cells. ns: no significance between

non-starved and starved cells. (**d**) Transmission Electron Micrograph (TEM) tomogram of ultrathin cryosections of ATG16L1 knock out cells expressing WIPI2-CAAX. Plasma membrane and thin cortical ER are color coded as shown in the schematic drawing. Scale bar = 200 nm. (**e**) PREM image of an unroofed cell expressing WIPI2-CAAX, ATG16L1 and LC3B. Arrowheads indicate membrane cups that are formed at omegasome-like membranes (W). Patches of plasma membrane are indicated by asterisks. Scale bar = 1µm. Confocal images of ATG161L1 KO cells expressing WIPI2-CAAX, GFP-LC3B and mCherry-tagged ATG16L1^{230} (**f**), ATG16L1^{264} (**g**), ATG16L1^{307} (**h**) and ATG16L1^{FL} (**i**). Merged GFP (green) and mCherry (red) images are shown. Confocal images of the corresponding single channels are shown in **Extended Data Figure 6b**. Scale bar = 5µm. (**f-i**) The high magnification PREM views show characteristic membrane deformations of unroofed ATG16L1 KO cells expressing WIPI2-CAAX, LC3B and HA-ATG16L1 variants as indicated. W denotes omegasome-like membranes from which cups emerge, * indicates regions in which the plasma membrane is visable. Scale bars = 1 µm and 200 nm (insets).

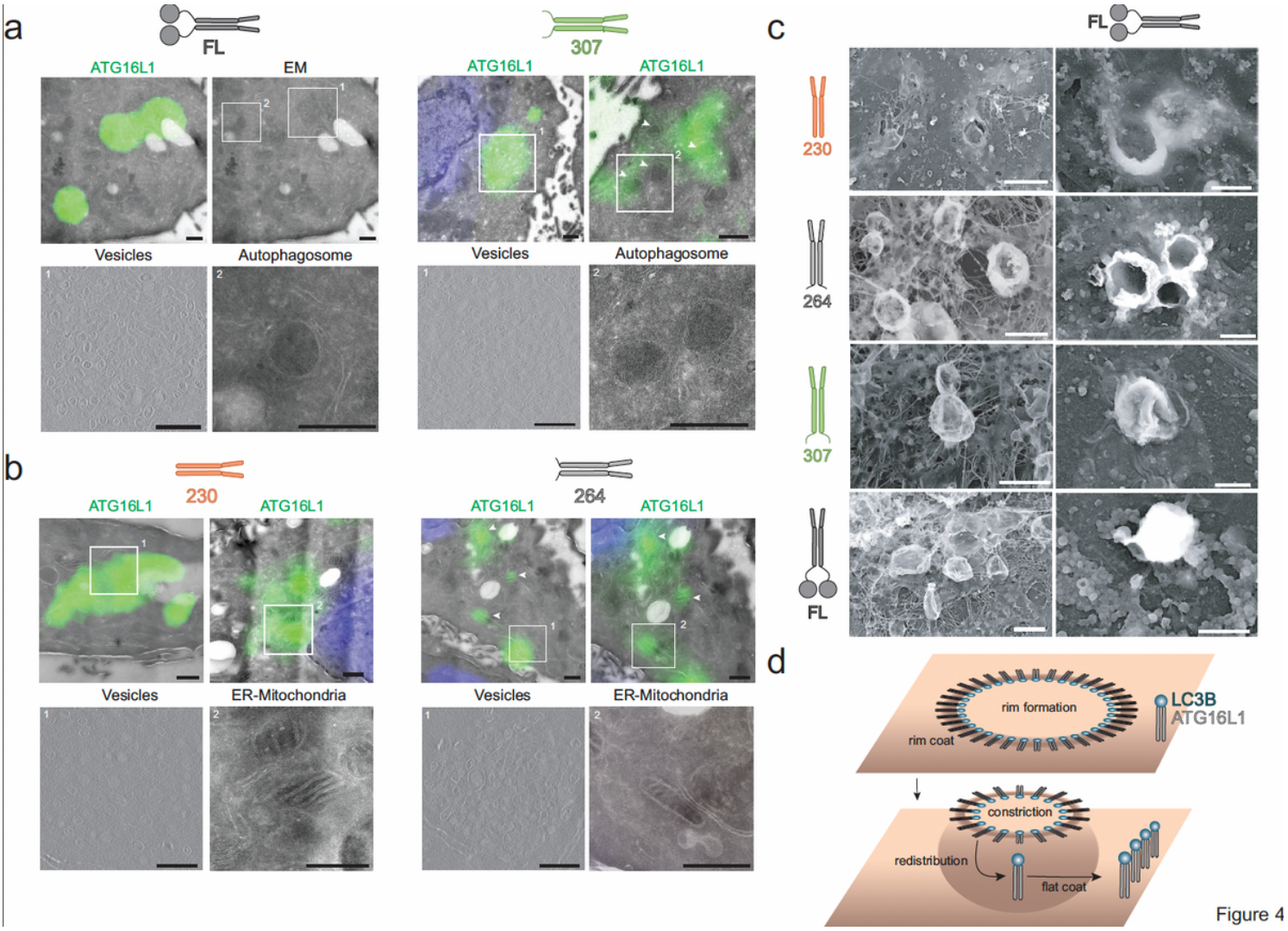

Figure 4

Figure 4

Formation of membrane cups and autophagosomes by ATG16L1 variants.

Correlative light electron microscopy images of cells expressing HA-tagged ATG16L1^{FL} or ATRG16L1^{307} (**a**) and ATG16L1^{264} or ATG16L1^{230} (**b**) in ATG16L1 knock out cells, labeled with anti-HA primary and Alexa488 labeled secondary antibody. Overview EM images in the top panel with superimposed fluorescence of ATG16L1 variants (green) and nucleus (blue). Scale bars = 1 µm. The corresponding insets show ATG16L1 vesicles and autophagosomes (**a**) or ER-mitochondria contact sites (**b**). Scale bars = 100 nm (**c**) Comparison of endpoints of cup formation as shown in high magnification PREM views of unroofed ATG16L1 KO cells expressing WIPI2-CAAX, LC3B and HA-ATG16L1^{230}, HA-ATG16L1^{264}, HA-ATG16L1^{307} and HA-ATG16L1^{FL} (left panel, scale bars = 1 µm) with intermediate of cup formation in PREM views of ATG16L1 KO cells expressing WIPI2-CAAX, LC3B and HA-ATG16L1^{FL} (right penal, scale bars = 500 nm). (**d**) Model of cup formation. ATG12–ATG5-ATG16L1 complexes self-assemble into ring-like structures that bend membranes into rims. Cups appear to evolve from membrane rims by remodeling the donor membrane that coincide with the formation of extended membrane coats in vitro.

Supplementary Files

This is a list of supplementary files associated with this preprint. Click to download.

- SupplementaryInformation.docx
- TableS1SourcedataFINAL.xlsx
- TableS2MMFINAL.xlsx
- ExtendedDataFigure1.pdf
- ExtendedDataFigure2.pdf
- ExtendedDataFigure3.pdf
- ExtendedDataFigure4.pdf
- ExtendedDataFigure5.pdf
- ExtendedDataFigure6.pdf
- ExtendedDataFigure7.pdf
- ExtendedDataFigure8.pdf
- MovieS1LifeconjugationLC3BtoGUVs.avi
- MovieS23DreconstructedGUVwithbuds.mp4
- MovieS3ATG16L1fulllengthinvitroURupmc121suitel131.avi
- MovieS4307invitromovieURupmc121suiteH66.avi
- MovieS5EMofcorticalER.mp4
- MovieS6ATG16L1FLmovieURupmc129E1520t.avi

- MovieS7230invivoURupmc129E1450tmoviev2.avi
- MovieS8FLSubtomo.avi
- MovieS9307tomovesicles.avi
- MovieS10264tomovesicles.avi
- MovieS11230tomovesicles.avi
- MovieS12tomo3moviestogether5fpscolor.avi